Highly Compact Swing Assistive Knee Prosthesis Integrating Active and Passive Hydraulic Systems

IEEE Access
Multidisciplinary | Rapid Review | Open Access Journal

Received 13 March 2025, accepted 28 April 2025, date of publication 7 May 2025, date of current version 16 May 2025.

Digital Object Identifier 10.1109/ACCESS.2025.3567881

RESEARCH ARTICLE

Highly Compact Swing Assistive Knee Prosthesis Integrating Active and Passive Hydraulic Systems

MARCO PULITI[1], (Student Member, IEEE), FEDERICO TESSARI[2], RENATO GALLUZZI[3], (Senior Member, IEEE), NICOLA AMATI[4], ANDREA TONOLI[4], AND MATTEO LAFFRANCHI[1]

[1]Rehab Technologies INAIL-IIT Laboratory, Italian Institute of Technology, 16163 Genoa, Italy
[2]Laboratory for Biomechanics and Human Rehabilitation, Massachusetts Institute of Technology, Cambridge, MA 02139, USA
[3]School of Engineering and Sciences, Tecnologico de Monterrey, Mexico City 14380, Mexico
[4]Center for Automotive Research and Sustainable Mobility (CARS), Politecnico di Torino, 10129 Turin, Italy

Corresponding author: Renato Galluzzi (renato.galluzzi@tec.mx)

This work was supported by Istituto Nazionale per l'Assicurazione contro gli Infortuni sul Lavoro (INAIL) under Grant PR19-PAI-P1–HyperLEG.

ABSTRACT This work proposes a novel partially powered knee prosthesis to give full support to swing related activities. It represents a technological step forward when compared to microprocessor-controlled knees. The device is based on the electro-hydrostatic actuation principle, combined with the use of a series rotary valve to aid during dissipative phases. Another key feature is the backdrivability enabled by a directly coupled fluid-based actuation principle. To this end, we present a compact design that is subsequently built and tested experimentally with an able-body adapter to simulate a real-case scenario of level walking and stair tasks. Results are compared with the features of existing commercial and research devices. To the best of the authors' knowledge, the proposed prosthesis is the most compact electro-hydrostatic swing assistive device with the potential to improve the walking gait, for instance by increasing toe clearance and likely reducing the occurrence of stumbling or falling events. Additionally, the prototype enables stair ascent in a step-over fashion, a capability generally unattainable with commercial microprocessor-controlled knees.

INDEX TERMS Amputation, electro-hydrostatic actuation, knee prosthesis, mechatronics.

I. INTRODUCTION

The ability to perform various types of gait and locomotion patterns is an essential characteristic for a healthy and functional life. Two of the most common gaits, walking and climbing stairs, are characterized by distinct phases: a standing phase and a swinging phase. During the stance phase, the limb remains in contact with the ground and is progressively loaded with the subject's weight. The limb is responsible for propelling the body toward desired goals, such as moving forward during walking or forward and upward during stair climbing. In contrast, the swing phase is the portion of gait during which the limb is not in contact with the ground. Each individual exploits a controlled ballistic movement to prepare the leg for the following contact [1]. The cyclic alternation of these phases generates the locomotion pattern [2].

For individuals with amputation, particularly those with a transfemoral amputation, restoring functional gait using prosthetics is a crucial and complex challenge [3], [4], [5]. From a mechanical perspective, a prosthesis must achieve two contrasting goals. During stance, it needs to generate high braking and active torques at relatively low speeds. During swing, it should operate at higher speeds, produce small torques, and exhibit low impedance, making it highly back-drivable. In terms of locomotion, the goal is to improve the quality of life of amputees. One approach to achieve this goal is to enable individuals with amputation to maintain as much 'agency' as possible over the device. Agency refers to the user's ability to directly influence the prosthesis' behavior.

To address these challenges, three categories of knee prostheses have been developed for transfemoral amputees:

The associate editor coordinating the review of this manuscript and approving it for publication was Jingang Jiang.

passive, fully powered, and semi-active. Passive devices typically use hydraulic dampers with fixed characteristics [6], [7]. Greater adaptability can be achieved by incorporating electronic valves in the so-called microprocessor knees (MPKs), allowing variable, passive impedance to support diverse activities. Low impedance is suitable for swing activities, whereas descending activities, such as sitting down, require high damping torques [8], [9].

A major limitation of MPKs is their inability to exert positive power at the knee joint. This capability is crucial when the forward natural dynamics are insufficient to drive the prosthesis, such as during slow walking, stair climbing, or when attempting to increase foot clearance to avoid an obstacle. Although reducing internal friction in MPKs could address this issue, activities like climbing stairs or standing up demand significant power, which cannot be provided passively. Given this limitation, prosthetic users usually employ unnatural movements, such as lifting their affected hip [10]. These unnatural compensation mechanisms are detrimental to individuals, as they often lead to comorbidities, such as low back pain and osteoarthritis on the non-affected side [11].

The state of the art proposes fully powered devices to overcome these limitations [12], [13], [14], [15], [16], [17], [18], [19], [20]. They use actuation units to replace passive valves, typically involving an electric motor and a suitable transmission. The motor size and transmission ratio can be chosen to achieve the required output force in a compact, self-contained package. They are typically designed to replicate the full spectrum of locomotion activities and have been used to improve power-draining tasks [21], [22], [23], [24], [25]. These studies have concluded that providing active power is essential to create a more biomimetic movement.

Although beneficial for some locomotion tasks, fully powered systems may suffer from poor backdrivability and a substantial reflected inertia. The former is typically caused by mechanical friction, particularly in the transmission, while the latter results from the high transmission ratios needed to meet the active torque demands during the stance propulsion phase.

To overcome the limitations of both fully-powered and passive devices, semi-active knee prostheses have been proposed [26], [27], [28], [29], [30]. These devices aim to strike a balance between functionality and usability. They typically use contained actuating units with low transmission ratios, which inherently enhance backdrivability and reduce coupled inertia. This improves the range of low-impedance dynamics the prosthesis can provide, potentially promoting a more natural swing motion during gait. Nevertheless, these improvements often imply a lower maximum output torque, limiting the assistance during the propelling phases of gait. Within this category, most systems exploit electromechanical actuation, typically using electric motors, coupled with transmission systems such as planetary gears or harmonic drives for rotary actuation, or ball and lead screws for linear actuation. These actuators are often paired with passive, controllable hydraulic systems, such as dampers and hydraulic valves. Actuators and dampers can be either rigidly coupled or clutched to the artificial knee joint.

While electromechanical systems have shown potential in the most relevant locomotion activities [31], [32], [33], [34], they may be limited by the drawbacks of pure electromechanical transmissions, including friction, noise and vibrations. Electro-hydrostatic actuation offers a potential alternative to electro-mechanical systems by replacing the mechanical transmission with a hydraulic one, such as a pump. This approach can overcome the limitations of electromechanical systems. Hydraulic-powered prostheses have been proposed for the ankle joint [35], [36], and similar concepts are being explored at the knee level [16], [30].

Our group has led the development of an electro-hydrostatic semi-active knee prosthesis, combining an electric motor with a gerotor pump, a linear hydraulic cylinder, and a flow-control valve. In previous works [37], [38], [39], we presented detailed modeling and design strategies aimed at maximizing system integration, enhancing backdrivability, reducing noise and weight, while providing sufficient active support to improve swing capabilities and offer partial support during stance phases. More recently, we presented a study detailing the design, manufacturing, and benchtop testing of the prosthesis components [40].

In this work, we present the fully integrated version of the electro-hydrostatic knee prosthesis and demonstrate its potential as a competitive alternative to electro-mechanical solutions for assisting gait in transfemoral amputees. This paper showcases how dedicated design methodologies, custom manufacturing solutions, and tailored control strategies can result in a compact, lightweight, and backdrivable device to assist knee flexion during swing phases of multiple gait activities. The prosthesis performance is evaluated on an able-bodied subject to simulate a near-real application scenario.

II. REQUIREMENTS

In this section, we summarize the main biomechanical and mechatronic requirements that a swing assistive knee prosthesis should fulfill.

A. BIOMECHANICS

Considering an adult male subject from the 50th statistical percentile with a body mass of 75 kg, the target mass of the prosthesis is set to $m_p \leq 3.5$ kg i.e., 4.7 % of the subject's mass. Although the knee is intrinsically a constrained spherical joint, a linear actuation mechanism is adopted, as it allows more uniform mass and volume distribution along the patient's body. Linear motion will be then converted to a suitable rotation at the knee joint using an inverted slider-crank mechanism, with a maximum range of motion of 110° to enable tasks like kneeling or sitting down [41].

B. POWER

To quantify energy consumption, healthy subject measurements were used. The most demanding tasks—knee yielding and stairs descent—demand maximum impedance torque of 135 N m, 400 W of power and 100 N m s/rad of damping for a 100-kg patient [42]. For swing motion, a less demanding task, 1 N m s/rad is a sufficient amount of damping [8] that can be attained passively. In terms of responsiveness, the actuator must be able to switch from these two limit damping values in less than 100 ms, which represents the average period between heel strike and foot flat [43].

In terms of autonomy, a battery pack must be integrated with the actuator. It must provide at least a full day of use, implying 3000 ± 1800 steps/day [44] and the power drawn by auxiliary devices (microcontrollers, sensors, power stage units, etc.).

C. ACTUATION

The human leg can be represented as a double pendulum mechanism. Assuming a leg with an actuated prosthetic device, the equilibrium of momenta at the knee is achieved through

$$\tau_{k,p} \approx \pm\tau_g + \tau_i + \tau_p \tag{1}$$

where $\tau_{k,p}$ is the passive contribution of the knee, a function of the flexion (+) or extension (−) gravitational torque (τ_g), the inertial torque (τ_i), and the prosthesis passive torque (τ_p).

Prosthesis design can be executed considering a null gravitational component and a worst-case (maximum) angular acceleration $\alpha_{k,max}$ of the rotating parts, thus yielding

$$\tau_i = \alpha_{k,max}\left(J_{leg} + N^2 J_{act}\right) \tag{2}$$

which considers the total inertia at the knee joint, divided into leg (J_{leg}) and actuator (J_{act}). Note that a transmission ratio N is included to reflect the actuator inertia to the knee. This value will be a function of the transmission mechanism sizing, as seen later. To limit the addition of unwanted inertial contributions, $J_{act}/J_{leg} \leq 0.1$ [45]. For a male patient of the 50$^{\text{th}}$ percentile, the shank will have its center of mass at 45% of the leg length $L_{kf} = 0.5$ m [46]. Furthermore, an angular acceleration of 100 rad/s^2 can be expected at the knee [41]. Thus, the inertial torque contribution can be estimated as

$$\tau_i = 1.1\alpha_{k,max} m_p \left(0.45\, L_{kf}\right)^2 \cong 20\,\text{N m} \tag{3}$$

Finally, swing activities involve a maximum angular speed of 7 rad/s and 110 W of active power. A list of the device requirements appears in Table 1.

TABLE 1. Prosthesis design requirements.

Description	Symbol	Value
Maximum swing torque	$\max(\tau_{k,a})$	20 N m
Maximum knee speed	$\max(\omega_k)$	7 rad/s
Maximum active power	$\max(P_{k,a})$	110 W
Knee range of motion	$\Delta\theta_k$	110°
Maximum prosthesis mass	$\max(m_p)$	3.5 kg
Maximum knee resistive torque	$\max(\tau_{k,r})$	135 N m
Maximum damping	$\max(\beta)$	100 N m s/rad
Minimum damping	$\min(\beta)$	1 N m s/rad

III. DESIGN AND ASSEMBLY

To attain the outlined specifications, the proposed active prosthesis relies on an electro-hydrostatic actuator (EHA) and a series variable-orifice valve. The conceptual layout of this system and a cross section of the assembly are illustrated in Fig. 1. The actuation is based on an inverted slider-crank mechanism that converts the linear displacement of a hydraulic cylinder into knee rotation. The force exerted or absorbed can be controlled through a motor-pump unit coupled to both chambers of the cylinder. One of the two hydraulic lines presents a motorized variable orifice in series that can control the hydraulic impedance of the cylinder without exerting active power to the system.

A. ELECTRO-HYDROSTATIC ACTUATOR

The EHA is constituted by an electric machine (brushless motor) and a fixed-displacement (gerotor) pump sharing the same shaft. Two lines connect the hydraulic pump to a cylinder with a piston. The selection of the cross section of this piston is usually critical, as slight positive variations often lead to significant actuator bulkiness. In this case, a piston area $A_p = 3.78\,\text{cm}^2$ was selected to bound the maximum pressure of the hydraulic circuit below 50 bar, while allowing integration without interference inside the prosthesis body.

The gerotor machine—adopted for its compactness and contained noise—has two gearing elements with n and $n+1$ teeth, respectively. The smaller gear rotates eccentrically inside the outer gear. Both gears rotate in the same direction, thus guaranteeing a very low relative speed with a pure rolling motion i.e., no sliding among the surfaces. Epitrochoidal gear profiles have been designed through a multi-objective evolutionary genetic algorithm [47], [48], which aims at finding a suitable trade-off between the overall efficiency of the device and its envelope [49]. This method evaluates the performance of the hydraulic machine at the most critical impedance (see Section II-B). To match motor torque with knee torque, a target gerotor volumetric displacement of the pump $D_p = 1.25\,\text{cm}^3$/rev was achieved with an outer gear outside diameter of 26 mm and an axial thickness of 13 mm. Considering the volumetric displacement and the piston cross section, the actuator transmission ratio is governed by

$$N = \frac{A_p}{D_p} N_{leg} \tag{4}$$

where N_{leg} is the transmission ratio of the inverted slider crank mechanism. In static conditions and considering an active sign convention, motor and knee active torque (τ_m, $\tau_{k,a}$), as well as motor and knee speed (ω_m, ω_k), are

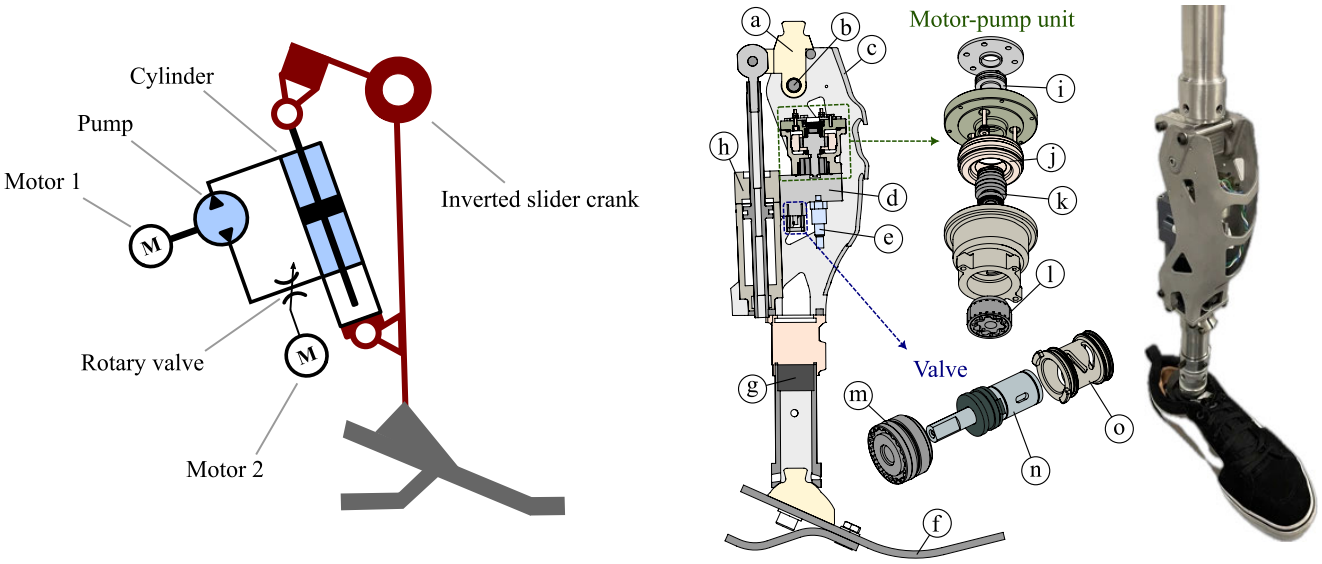

FIGURE 1. Electro-hydrostatic actuator for knee prosthesis (left). Actuation unit and rotary valve are connected in series to the linear hydraulic cylinder. Knee prosthesis prototype assembly (right): (a) pyramidal joint, (b) slow shaft with encoder, (c) frame, (d) manifold, (e) pressure sensor [×2], (f) passive foot-ankle, (g) load cell, (h)hydraulic cylinder. Motor-pump: (i) angular sensor, (j) stator, (k) rotor, (l) pump gears. Valve: (m) cap, (n) spool, (o) sleeve.

related through N:

$$\begin{cases} \tau_{k,a} = N\tau_m - N\tau_f \\ \omega_m = N\omega_k - \omega_\ell \end{cases} \tag{5}$$

where τ_f and ω_ℓ denote the friction torque and leakage angular speed, respectively, both seen from the motor standpoint.

To achieve this EHA design proposal, the resulting actuator was equipped with a frameless brushless motor, the TQ RoboDrive ILM38 × 06. This allows for a seamless integration with the rest of the system, guaranteeing a continuous torque up to $\tau_{m,cont} = 100\,\text{mN m}$, and a peak value $\tau_{m,pk} = 320\,\text{mN m}$. This latter feature enables a maximum swing active torque of 20 N m at the knee. With a maximum speed $\omega_{m,pk} = 10.5\,\text{kr/min}$, the machine can guarantee actuation within the established requirements. As indicated previously, both the electric motor and the pump share the same shaft. To avoid the addition of a rubber seal, the stator and the rotor of the electric machine operate immersed in oil.

The series hydraulic valve should operate as a restrictor that provides a variable impedance in the EHA circuit. Its role is to yield a resistive contribution to aid the EHA motor and pump when its braking torque is not enough to fulfill the impedance requirements of the knee motion task.

From a practical perspective, the valve is a custom design with a rotary spool and a sleeve. Angular rotation θ is provided by a Faulhaber 1016 SR DC motor and a 64:1 planetary gearbox. Variable grooves are obtained through the precise overlapping between the spool and the sleeve bodies. From the behavior of a hydraulic orifice, a nonlinear relationship between damping force F and linear speed v is a function of the equivalent groove orifice area A, which in turn depends on the valve opening θ:

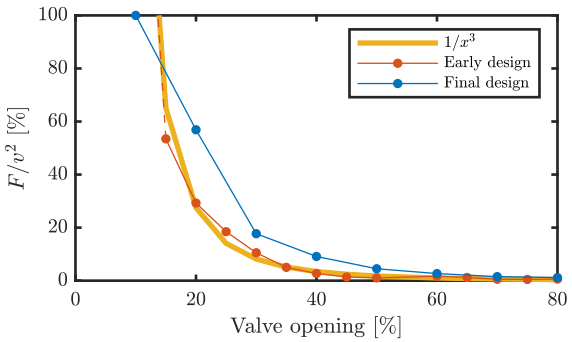

FIGURE 2. Characterization of two orifice valves. An early design based on off-the-shelf components shows a strongly nonlinear ($1/x^3$) equivalent quadratic damping F/v^2, undesirable for control purposes. The final design reduces this nonlinearity.

$$F \propto \frac{v^2}{A(\theta)^2} \tag{6}$$

The nonlinearity in (6) impedes a precise regulation of the hydraulic load. Specifically, at high braking torques and low speeds, the valve operates almost closed and the damping behavior is extremely sensitive to the valve rotation angle. By converse, low hydraulic load phases demand a large angular stroke that would be difficult to attain within the desired actuation bandwidth. This undesired effect would worsen as A increases with θ. Many off-the-shelf valves display this behavior, as depicted in Fig. 2, for which we found an experimentally determined relationship: $F \propto v^2/\theta^3$.

B. ROTARY HYDRAULIC VALVE

To minimize the nonlinear force response with respect to the valve rotation, a custom valve is designed. Equation (6)

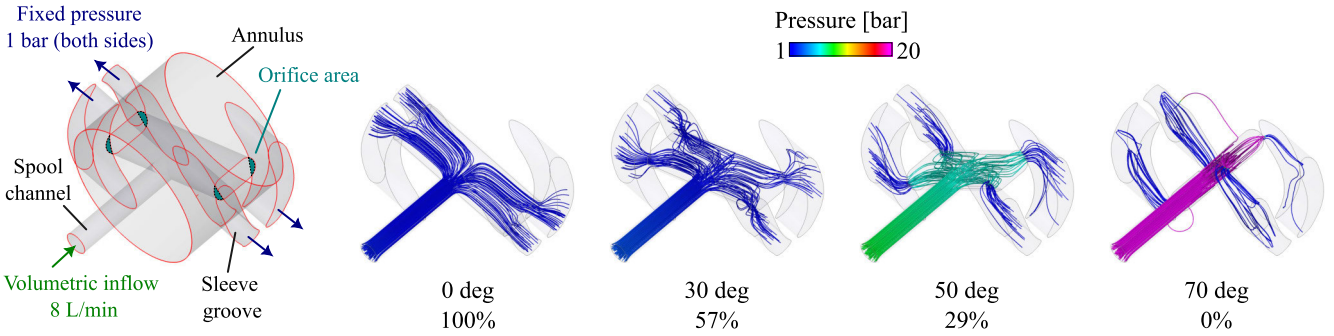

FIGURE 3. Variable-orifice valve simulation setup and results for different opening values. Streamlines are colored according to the pressure of the fluid.

suggests that A should change regressively as function of the spool rotation, according to $A \propto \theta^{-1/2}$, to achieve the linear relation $F \propto v^2\theta$. However, this exact relation is only based on the approximation of the orifice-plate expression (6) and impractical from a manufacturing perspective. For these reasons, the cross-sectional geometry of A is defined through a machinable cubic spline, refined with the aid of computational fluid-dynamic (CFD) analyses in Simerics Pumplinx. Considering mineral oil properties and a thin annulus region between the spool and the sleeve ($g_{rad} = 10\,\mu\text{m}$), CFD models were executed with flow rate values between -10 to $10\,\text{L/min}$ (21 values) and opening angles between zero and 70 deg, for a total of 210 runs.

Figure 3 illustrates the valve structure and the simulation boundary conditions. It also shows simulation results for an inflow of $8\,\text{L/min}$ at four different opening values. Streamlines indicate the fluid flow patterns; their color denotes the pressure delta generated by the orifice. It is observed that the pressure delta is mostly generated across the orifice area, which varies with the opening angle between the spool and the sleeve of the valve.

Figure 2 also shows results of the performance of the newly designed valve with improved groove shapes in comparison to a commercial valve. An improvement in linearity of more than 1200 % can be observed for a valve opening range between 10 % and 60 %, based on a comparison of minimum and maximum rate of change of damping force for valve opening ($\partial F/\partial\theta$) within this range. It is worth noting that with the impedance characteristic of the early design valve, it was not possible to evaluate force responses below 20 % of valve opening. The amount of required pressure drop to attain those working points was beyond the testbed pumping capability. This strongly suggests a much steeper damping curve compared to the new design.

C. PROTOTYPE ENVELOPE

The final prototype assembly can be subdivided into motor-pump, cylinder and valve bodies, for a total actuator mass of 900 g. Additional contributions are added by the knee joint assembly (400 g), a load cell (100 g), an electronic control unit (120 g), and a battery pack (350 g). The total

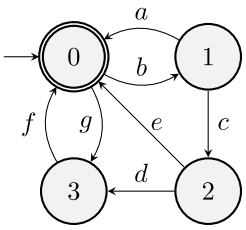

Transition	Condition
$a: 1 \to 0$	Thigh behind torso ($\theta_t < 0$) $\wedge$ Prosthesis load $<15\,\%$ weight $\wedge$ Knee angle $<10°$
$b: 0 \to 1$	Prosthesis load $>15\,\%$ weight
$c: 1 \to 2$	Prosthesis load $<7.5\,\%$ weight
$d: 2 \to 3$	Knee speed sign change $\wedge\ \omega_k < 0$
$e: 2 \to 0$	Prosthesis load $>40\,\%$ weight
$f: 3 \to 0$	Prosthesis load $>40\,\%$ weight $\wedge$ Knee angle $<2°$
$g: 0 \to 3$	Prosthesis load $<10\,\%$ weight $\wedge$ Knee angle $>10°$

FIGURE 4. Prosthesis finite-state machine for walking and stair tasks. States: (0) stance, (1) pre-swing, (2) swing flexion, (3) swing extension.

mass of the prosthesis is $m_p = 2.15\,\text{kg}$, thus fulfilling initial biomechanical requirement of $m_p \leq 3.5\,\text{kg}$. To give means of comparison, the C-Leg from Ottobock and the Genium X3 are two MPKs that weigh 1.5 and 1.8 kg, respectively. Although our design is heavier, it brings the additional benefit of active power compensation when compared to an MPK, with a mass increase of only 30%. In contrast, Ossur's Power Knee, a fully active device, is 49% heavier with a mass of 3.2 kg.

In terms of build height, our prototype is 240 mm, thus guaranteeing proper fit with a wide diversity of patients. Ottobock's C-Leg has a larger build height of 289 mm in the best of cases [50].

The knee-center to top pyramid distance of our prototype is 53 mm. This distance must be sufficiently short to fit patients with more distal amputations. Further evaluations are required to assess which percentile of above-knee amputations can be fit with our prosthesis.

IV. PROSTHESIS CONTROL: WALKING AND STAIRS

For control purposes, the prosthesis is equipped with two sensors to measure the pressure in the two hydraulic lines of the EHA. They allow estimating the knee torque. A load cell determines the reaction force between the prosthesis and the ground. Additionally, the angular motion of the knee joint is measured using a magnetic encoder. Finally, an inertial measurement unit allows estimating thigh and shank motion in space.

Since the focus of this work is on technology rather than controller design, the chosen controller is based on

well-known and proven methods. For this purpose, a finite state machine (FSM) is adopted and has been tuned to yield satisfactory walking results. The FSM is shown in Fig. 4, and features four discrete states: stance (0), pre-swing (1), swing flexion (2) and swing extension (3). During walking, the controller cycles sequentially through states, according to the conditions presented in Fig. 4. States are defined as follows:

1) *Stance*: Valve opening 20 % to yield proper damping for stance flexion (0.75 N m s/(rad kg)); EHA back-driven;
2) *Pre-swing*: Valve opening 80 %; EHA backdriven;
3) *Swing flexion*: Valve opening 100 %; EHA actively controlled;
4) *Swing extension*: Same as swing flexion.

The active-side controller is based on recently published works [31], [32], in which the control strategy has been validated on a different device [27]. Here, it has been adapted to match the features of the described prototype. The EHA controller comprises an outer impedance loop that imposes a desired torque

$$\tau_d = \beta_d \omega_k^n + \tau_0 \,\mathrm{sign}(\omega_k) \tag{7}$$

being β_d the desired damping to compensate, ω_k the knee angular speed, $n \geq 1$ representative of the damping model (e.g., linear or turbulent) and τ_0 the static friction torque identified in preliminary tests. Furthermore, no stiffness contribution is considered and the desired angular speed is set to zero. No virtual inertia was imposed to avoid the control robustness issues typically associated with inertia shaping. Impedance controllers, and their variations (e.g., admittance), have been extensively used in contexts requiring relevant physical interaction, such as prosthetics, thanks to their capability to provide a programmable compliant behavior [51].

Specifically, the goal is to partially compensate for the prosthesis homogeneous dynamic behavior without imposing an unnatural movement at the joint. Thus, by initiating an inertially coupled movement through the hip, the user retains agency over the prosthesis as a natural swing is essentially facilitated.

Furthermore, the controller incorporates two additional cascade loops. A proportional torque loop addresses friction and other nonlinear effects at the knee joint. This loop outputs desired current setpoints, which are fed to the field-oriented control (FOC) of the motor. Both loops operate in the embedded microcontroller at frequencies of 1 kHz and 20 kHz, respectively. The high-level control and the finite state machine run in a MATLAB-Simulink real-time environment at 200 Hz and communicate through CAN with the embedded microcontroller.

Finally, the same FSM is employed for both stairs ascent and descent, with two distinctions. During stair descending, the FSM cycles exclusively between states 0 and 3, and the valve position is adjusted during stance to accommodate

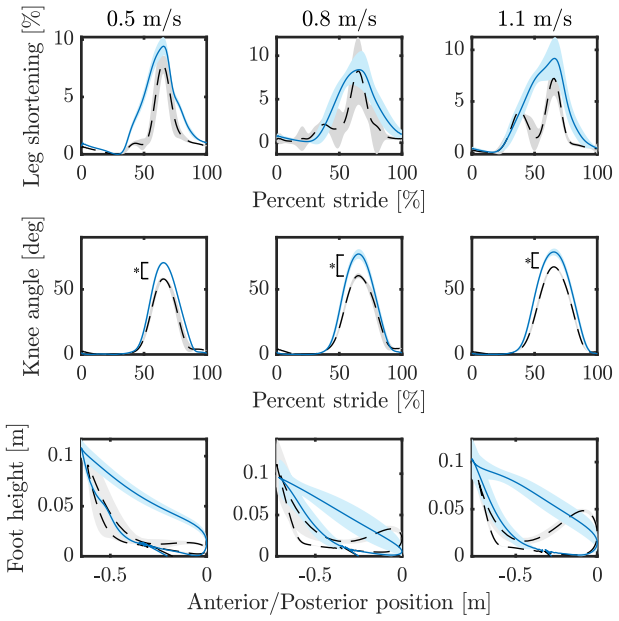

FIGURE 5. Prosthesis walking results. Black, dashed curves represent commercial results. Blue, solid curves represent prototype results. Bands define ±1 standard deviation from the mean. Statistical significance is marked with an asterisk.

the changing transmission ratio caused by significant knee yielding compared to the walking stance phase. On the other hand, during stair ascent, the FSM cycles through all four states, utilizing a different swing extension controller. Specifically, a shank angle virtual spring with a set point at 0 is introduced to create a soft stop at vertical shank position. The control law is of the form

$$\tau_d = \beta_d \omega_k^n + \tau_0 \,\mathrm{sign}(\omega_k) - K_p(\theta_s)\theta_s \tag{8}$$

In this setup, $K_p(\theta_s)$ is gradually increased within 25 ms after the shank angle θ_s falls below 5°. This added term prevents the prosthesis from impacting the step during stair ascent. A higher homogeneous dynamic cancellation is considered since the hip's dynamic contribution is lower than in walking. Regardless from the control mode, the EHA controller is the same for all the stair ascent gaits.

V. PROSTHESIS CHARACTERIZATION

Tests were conducted to validate the prosthesis performance in a close-to-real scenario: a healthy individual equipped with an able-body adapter, replicating the 50$^{\text{th}}$ percentile height of a prosthetic limb. A representative video of the walking and stairs trials is included as supplementary material.

A. WALKING EXPERIMENTS

Walking experiments are carried out to compare the prototype developed with the commercial Ottobock C-Leg 4 prosthesis. Tests are conducted on an AMTI split-belt, force-instrumented treadmill at three representative walking speeds: 0.5 m/s (slow), 0.8 m/s (self-selected), and 1.1 m/s

TABLE 2. Walking results: metrics average value.

Variable	Walking speed [m/s]					
	0.5		0.8		1.1	
	C	P	C	P	C	P
Peak knee angle [°]	58	70.5	60.5	77.2	67.3	78.7
Peak leg short. [%]	7.8	9.4	8.2	8.4	7.2	9.2
Stride length [m]	0.62	0.65	0.72	0.71	0.73	0.77
Stride time [s]	1.24	1.3	0.9	0.89	0.67	0.7
Peak current [A]	–	7.8	–	9.3	–	10.3
Autonomy [strides]	–	9350	–	5400	–	4260

C: commercial device, P: prototype

(fast). Kinematic data for the lower extremities are recorded using a Vicon infrared motion capture system. Each trial involves a 90 s walking duration, beginning with the use of the commercial device.

Figure 5 displays the results for both commercial and prototype prostheses, segmented by strides, across three walking speeds. The data depicted represent averages over approximately 20 strides, with colored bands indicating plus/minus one standard deviation from the average. The top row of Fig. 5 illustrates the percentage of leg shortening, representing the vertical distance between pelvis and toe markers throughout the stride. A null (zero) percentage indicates the maximum distance between the markers. At 0.5 m/s and 1.1 m/s, results show a higher leg shortening when testing with the prototype. Results at 0.8 m/s reveal similar percentages between the two devices under testing.

The prototype consistently demonstrates higher peak knee flexion compared to the commercial prosthesis, in all three scenarios. The bottom row of Fig. 5 illustrates foot movement in the sagittal plane. At both 0.5 and 1.1 m/s, the prototype achieves a greater maximum foot height than the commercial prosthesis, with a comparable stride length.

Table 2 provides a summary of key findings for both commercial and prototype prostheses at various walking speeds. Pair-wise t-tests are conducted to assess any significant difference in the peak value of the knee angle between the commercial and prototype solutions, at each walking speed. Results reveal $p < 0.001$ in all three walking conditions.

Moreover, an energetic analysis is conducted to characterize the autonomy of the prosthesis. Taking into account electric motor, control and power stage losses, the average power consumption per stride is 27.62, 47.5, and 60.58 W for the three investigated walking speeds, respectively.

B. STAIRS EXPERIMENTS

Stairs experiments are exclusively conducted with the prototype prosthesis. However, various studies have presented stair ascent and descent kinematic data for commercial MPKs [52], [53]. Experiments are carried out on a six-step staircase, considering two ascending gaits: step to (ST) and step over (SO) step. ST represents the conventional gait for transfemoral amputees, whereas SO is the common gait observed in able-bodied individuals. Results for knee angle and exerted torque are presented in Fig. 6. In both ascending gaits, a large peak knee flexion is attained: 35° for ST and 39° for SO, as opposed to 5° and 10° with conventional MPKs, respectively [53].

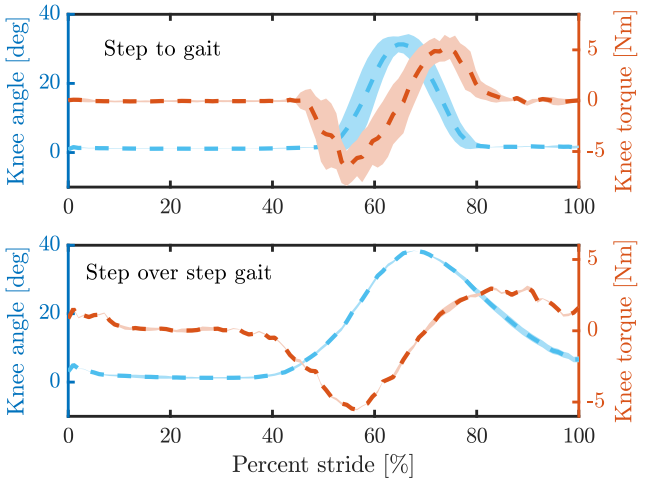

FIGURE 6. Stair ascent results using the developed prototype on an able-bodied subject. Two different step strategies are shown: step to gait (top) and step over step gait (bottom). Average knee angle (blue) is positive for increasing flexion. Knee torque (orange) is negative for increasing flexion. Bands define ±1 standard deviation from the mean.

Step clearance is achieved by applying torque at the joint, as detailed in Section IV. The peak torque values, 5.4 N m for ST and 7.2 N m for SO, correspond to the swing flexion state, with no assistance provided during the load-support phase.

VI. DISCUSSION

A. PROTOTYPE PERFORMANCE

With a mass of only 2.15 kg, our device falls into the partially powered prosthesis category with the objective of providing swing assistance in a variety of tasks. These functional features are achieved with a custom design combining EHA and a series rotary valve. The final prototype guarantees 2.6 N m s/rad of minimum viscous damping, with a nonlinear stiction force of only 38.5 N. In active mode, the device can track a sinusoidal motion reference with a peak flexion of 90°, a maximum angular speed of 49 r/min, and a maximum power draw of 52 W.

The finite state machine was able to reproduce the walking and stair climbing tasks and the impedance controller favored agency over the prosthesis. This means that the user can impose their own residual limb dynamics to the device. Walking tests were performed on an able-bodied user through a dedicated adapter at three different speeds (0.5, 0.8, 1.1 m/s), considering both the developed prototype and a commercial MPK. In all three scenarios, the peak knee flexion is consistently higher for the prototype compared to the commercial prosthesis. This is indicative of greater leg flexion in the prototype, as depicted in the middle row of Fig. 5. The bottom row of Fig. 5 depicts foot movement on the sagittal plane. At both 0.5 and 1.1 m/s, the prototype exhibits

TABLE 3. Comparison of key features across different prosthetic designs.

Feature	Prototype [40]	SCSA v2 [31]	Hybrid Utah [28]	HSAK [30]
Transmission type	Series hydraulic	Mechanical	Mechanical	Parallel hydraulic
Knee range of motion [°]	110	110	110	120
Prosthetic mass [kg]	2.15	1.8	1.68	2.68
Build height [mm]	230	238	N/A	258
Coulomb friction [N]	35	25	N/A	3
Inherent damping [N s/m]	1900	500	3R95	N/A
Back-drive torque [N m]	N/A	N/A	4.8	4.42
Reflected inertia [kgcm^2]	150	17	N/A	N/A
Transmission ratio (avg) [mm/rad]	37.5	22.5	150 ÷ 500	126 ÷ 174
Active torque [N m]	20	10	125	52

N/A: Data not available or not applicable.

a higher maximum foot height compared to the commercial prosthesis, while the stride length remains comparable. This result suggests an increased toe clearance, metric directly relatable to likelihood of stumbling or falling [54]. It is important to underline that while a greater foot height could reduce the risk of stumbling and falling, it might also induce a higher energy expenditure for the user. Future clinical evaluations should address this criticality.

Considering a 21.6 V pack with a capacity of 3350 mA h, the prosthesis can sustain 9350, 5400, and 4260 strides at the respective speeds. These values correspond to a range of usage from a maximum of 3 to a minimum of 1.5 days, taking into account the average number of steps per day performed by TFAs [44].

The prototype is also tested during stair tasks, showing promising results with a peak knee flexion of 39° during a step-over-step ascending gait. Comparative literature findings for MPKs typically report minimal knee flexion during ST [52] and the inability to perform a step-over-step (SO) gait. The Ottobock Genium is the sole commercial MPK capable of executing a SO gait, though requiring a non-natural movement initiation [53].

B. COMPARISON WITH OTHER PROSTHESIS TYPES

This work presents a prosthesis evolution with respect to its previous version [16]. Although the previous-generation device covered a significant portion of the target gait cycle, low speed - high torque phases (i.e., stance) could not be compensated due to the intrinsic power limitations and compact size of the EHA. These shortcomings have been addressed in this design, by adding the series rotary valve.

The new prototype prosthesis has been benchtop validated in a previous work for both active and passive operating modes [40]. For sake of comparison, the most relevant results and how they compare to existing literatures [28], [30], and [31] are presented in Table 3.

The work by Li et al. features an hydraulic transmission [30], similar to our proposed prototype. However, differently from our design, their active hydraulic element (i.e., pump) acts in parallel to the spring-damper system. This could represents an advantage when exerting power towards the joint as the damper pressure drop can be bypassed. Conversely, when dissipating high power (i.e., during walking stance), the active side cannot be bypassed by the damper system. As such, it should provide most of such resistive power.

In their work, Lee et al. [27] propose a device with a similar mass (2.18 kg), but a more substantial height (278 mm) and a full-day autonomy. In contrast, our solution delivers higher swing torque (12.15 versus 7.5 Nm), with comparable power consumption. Furthermore, when tracking position setpoints, the proposed device exhibits more favorable responsiveness, with a tracking delay of 20 ms instead of $\sim$ 40 ms [27], at the cost of a larger command effort.

When compared to the most advanced fully powered prostheses in literature, our device presents similar mass to the prototype by Azocar et al. [13], which is slightly above the solution by Tran et al. [14]. In terms of build height and battery autonomy, all three devices are comparable. For backdrivability, the minimum damping by Tran et al. is significantly lower, (0.43 versus 2.6 Nms/rad). However, this latter value is suitable to compensate ballistic motion passively [8]. Unlike purely electromechanical technologies [13], [14], [27], the fluid-based transmission of EHAs is qualitatively perceived as smooth. This is due to the natural leakages inside the circuit and the viscous impedance introduced by the oil itself. Despite the presence of these losses, our device was able to reach full-day autonomy efficiently.

C. RESEARCH NOVELTY

Considering the presented results and comparison with existing alternatives, this research presents—to the best of our knowledge—the first and most integrated (2.15 kg in a compact envelope) design and validation (walking and stair climbing) of a swing assistive knee prosthesis using a fully-custom electro-hydrostatic actuation (EHA) with a in-series hydraulic valve.

The adopted serial architecture provides several advantages compared to other solutions. First, compared to parallel hydraulic designs (in which the valve is placed in parallel with the actuation), our design has an improved tolerance to faults since, in case of actuator failure, the series valve will still

be able to brake the knee motion, essentially behaving as a conventional MPK.

Moreover, compared to series electromechanical systems, no gear mechanisms are needed to convert the motion from the hydraulic to the mechanical domain, thus reducing losses and noise in the system. Electro-hydrostatic actuation also reduces the mechanical design coupling needs e.g., belts, chains, gears, since the actuation can be easily located anywhere in the prosthesis and connected to the final end-effector by means of dedicated hydraulic lines.

The implemented impedance-based controller demonstrated the ability to perform walking and stair climbing tasks while providing an intrinsically stable behavior thanks to the passivity constraint imposed by the control law. Moreover, the velocity driven control, aimed at enhancing user agency, aligns with recent neuroscientific findings that humans might encode their motion using descending velocity commands [55].

VII. CONCLUSION

This paper proposed a partially powered knee prosthesis based on electro-hydrostatic actuation principles, combined with the dissipative assistance of a series rotary valve. The design was custom developed to guarantee an elevated degree of integration. A dedicated prototype was built and tested, demonstrating active capabilities to match the swing phase of multiple knee motion tasks. Experiments were carried out on a healthy subject using an able-body adapter. These close-to-real use conditions showed improved performance when comparing the device to prominent MPK alternatives.

Further investigations will delve into the validation of the prototype on transfemoral amputee population. This aspect is fundamental to confirm the results obtained on healthy individuals. Furthermore, we will assess the finite state machine that controls the prototype under different operating conditions. The goal is to yield a robust actuator and enable clinical trials with amputee patients in the near future.

REFERENCES

[1] S. Mochon and T. A. McMahon, "Ballistic walking: An improved model," *Math. Biosciences*, vol. 52, nos. 3–4, pp. 241–260, Dec. 1980.

[2] A. D. Kuo and J. M. Donelan, "Dynamic principles of gait and their clinical implications," *Phys. Therapy*, vol. 90, no. 2, pp. 157–174, Feb. 2010, doi: 10.2522/ptj.20090125.

[3] R. E. Seroussi, A. Gitter, J. M. Czerniecki, and K. Weaver, "Mechanical work adaptations of above-knee amputee ambulation," *Arch. Phys. Med. Rehabil.*, vol. 77, no. 11, pp. 1209–1214, Nov. 1996.

[4] C. Gauthier-Gagnon, M.-C. Grisé, and D. Potvin, "Enabling factors related to prosthetic use by people with transtibial and transfemoral amputation," *Arch. Phys. Med. Rehabil.*, vol. 80, no. 6, pp. 706–713, Jun. 1999.

[5] T. Lencioni, I. Carpinella, M. Rabuffetti, A. Marzegan, and M. Ferrarin, "Human kinematic, kinetic and EMG data during different walking and stair ascending and descending tasks," *Scientific Data*, vol. 6, no. 1, p. 309, Dec. 2019.

[6] W. Liang, Z. Qian, W. Chen, H. Song, Y. Cao, G. Wei, L. Ren, K. Wang, and L. Ren, "Mechanisms and component design of prosthetic knees: A review from a biomechanical function perspective," *Frontiers Bioengineering Biotechnol.*, vol. 10, Sep. 2022, Art. no. 950110.

[7] M. A. Price, P. Beckerle, and F. C. Sup, "Design optimization in lower limb prostheses: A review," *IEEE Trans. Neural Syst. Rehabil. Eng.*, vol. 27, no. 8, pp. 1574–1588, Aug. 2019.

[8] J. Camargo, A. Ramanathan, W. Flanagan, and A. Young, "A comprehensive, open-source dataset of lower limb biomechanics in multiple conditions of stairs, ramps, and level-ground ambulation and transitions," *J. Biomechanics*, vol. 119, Apr. 2021, Art. no. 110320.

[9] S. Hood, M. K. Ishmael, A. Gunnell, K. B. Foreman, and T. Lenzi, "A kinematic and kinetic dataset of 18 above-knee amputees walking at various speeds," *Scientific Data*, vol. 7, no. 1, pp. 1–8, May 2020.

[10] V. J. Harandi, D. C. Ackland, R. Haddara, L. E. C. Lizama, M. Graf, M. P. Galea, and P. V. S. Lee, "Gait compensatory mechanisms in unilateral transfemoral amputees," *Med. Eng. Phys.*, vol. 77, pp. 95–106, Mar. 2020.

[11] D. C. Morgenroth, M. Roland, A. L. Pruziner, and J. M. Czerniecki, "Transfemoral amputee intact limb loading and compensatory gait mechanics during down slope ambulation and the effect of prosthetic knee mechanisms," *Clin. Biomechanics*, vol. 55, pp. 65–72, Jun. 2018.

[12] S. C. Culver, L. G. Vailati, and M. Goldfarb, "A power-capable knee prosthesis with ballistic swing-phase," *IEEE Trans. Med. Robot. Bionics*, vol. 4, no. 4, pp. 1034–1045, Nov. 2022.

[13] A. F. Azocar, L. M. Mooney, J.-F. Duval, A. M. Simon, L. J. Hargrove, and E. J. Rouse, "Design and clinical implementation of an open-source bionic leg," *Nature Biomed. Eng.*, vol. 4, no. 10, pp. 941–953, Oct. 2020.

[14] M. Tran, L. Gabert, S. Hood, and T. Lenzi, "A lightweight robotic leg prosthesis replicating the biomechanics of the knee, ankle, and toe joint," *Sci. Robot.*, vol. 7, no. 72, pp. 1–17, Nov. 2022.

[15] F. Sup, H. Atakan Varol, J. Mitchell, T. J. Withrow, and M. Goldfarb, "Preliminary evaluations of a self-contained anthropomorphic transfemoral prosthesis," *IEEE/ASME Trans. Mechatronics*, vol. 14, no. 6, pp. 667–676, Dec. 2009.

[16] F. Tessari, R. Galluzzi, A. Tonoli, N. Amati, L. De Michieli, and M. Laffranchi, "Knee prosthesis powered by a fully integrated and highly back-drivable electro-hydrostatic actuator," *Mechatronics*, vol. 91, May 2023, Art. no. 102972.

[17] B. E. Lawson, J. Mitchell, D. Truex, A. Shultz, E. Ledoux, and M. Goldfarb, "A robotic leg prosthesis: Design, control, and implementation," *IEEE Robot. Autom. Mag.*, vol. 21, no. 4, pp. 70–81, Dec. 2014.

[18] J. Zhu, C. Jiao, I. Dominguez, S. Yu, and H. Su, "Design and backdrivability modeling of a portable high torque robotic knee prosthesis with intrinsic compliance for agile activities," *IEEE/ASME Trans. Mechatronics*, vol. 27, no. 4, pp. 1837–1845, Aug. 2022.

[19] G. Fu, J. Zhu, Z. Wang, J. Mai, and Q. Wang, "Mechatronic design and implementation of a low-noise powered knee prosthesis with high backdrivability," *IEEE/ASME Trans. Mechatronics*, vol. 28, no. 6, pp. 3180–3190, Jun. 2023.

[20] T. Elery, S. Rezazadeh, C. Nesler, and R. D. Gregg, "Design and validation of a powered knee–ankle prosthesis with high-torque, low-impedance actuators," *IEEE Trans. Robot.*, vol. 36, no. 6, pp. 1649–1668, Jun. 2020.

[21] S. Cheng, C. A. Laubscher, and R. D. Gregg, "Automatic stub avoidance for a powered prosthetic leg over stairs and obstacles," *IEEE Trans. Biomed. Eng.*, vol. 71, no. 5, pp. 1499–1510, May 2024.

[22] C. G. Welker, T. K. Best, and R. D. Gregg, "Improving Sit/Stand loading symmetry and timing through unified variable impedance control of a powered knee-ankle prosthesis," *IEEE Trans. Neural Syst. Rehabil. Eng.*, vol. 31, pp. 4146–4155, 2023.

[23] T. K. Best, C. G. Welker, E. J. Rouse, and R. D. Gregg, "Data-driven variable impedance control of a powered Knee–Ankle prosthesis for adaptive speed and incline walking," *IEEE Trans. Robot.*, vol. 39, no. 3, pp. 2151–2169, Jun. 2023.

[24] G. R. Hunt, S. Hood, L. Gabert, and T. Lenzi, "Effect of increasing assistance from a powered prosthesis on weight-bearing symmetry, effort, and speed during stand-up in individuals with above-knee amputation," *IEEE Trans. Neural Syst. Rehabil. Eng.*, vol. 31, pp. 11–21, 2023.

[25] S. Hood, L. Gabert, and T. Lenzi, "Powered knee and ankle prosthesis with adaptive control enables climbing stairs with different stair heights, cadences, and gait patterns," *IEEE Trans. Robot.*, vol. 38, no. 3, pp. 1430–1441, Jun. 2022.

[26] B. G. A. Lambrecht and H. Kazerooni, "Design of a semi-active knee prosthesis," in *Proc. IEEE Int. Conf. Robot. Autom.*, May 2009, pp. 639–645.

[27] J. T. Lee, H. L. Bartlett, and M. Goldfarb, "Design of a semipowered stance-control swing-assist transfemoral prosthesis," *IEEE/ASME Trans. Mechatronics*, vol. 25, no. 1, pp. 175–184, Feb. 2020.

[28] T. Lenzi, M. Cempini, L. Hargrove, and T. Kuiken, "Design, development, and testing of a lightweight hybrid robotic knee prosthesis," *Int. J. Robot. Res.*, vol. 37, no. 8, pp. 953–976, Jul. 2018.
[29] J. Park, G.-H. Yoon, J.-W. Kang, and S.-B. Choi, "Design and control of a prosthetic leg for above-knee amputees operated in semi-active and active modes," *Smart Mater. Struct.*, vol. 25, no. 8, Aug. 2016, Art. no. 085009.
[30] Z. Li, Y. Han, C. Liu, H. Xiu, G. Wei, and L. Ren, "Design, manufacture, and experimental validation of a hydraulic semi-active knee prosthesis," *IEEE Trans. Neural Syst. Rehabil. Eng.*, vol. 31, pp. 1394–1404, 2023.
[31] D. M. Marsh, M. Puliti, and M. Goldfarb, "A swing-assist controller for enhancing knee flexion in a semi-powered transfemoral prosthesis," *IEEE Trans. Neural Syst. Rehabil. Eng.*, vol. 32, pp. 4052–4062, 2024.
[32] M. Puliti, D. M. Marsh, and M. Goldfarb, "Homogeneous dynamic control for stair ascent in a swing-assist knee prosthesis," *IEEE Trans. Med. Robot. Bionics*, vol. 6, no. 4, pp. 1637–1647, Nov. 2024.
[33] J. Lee and M. Goldfarb, "The effects of swing assistance in a microprocessor-controlled transfemoral prosthesis on walking at varying speeds and grades," *Wearable Technol.*, vol. 4, pp. e9-1–e9-11, Mar. 2023.
[34] J. Lee, S. King, M. Eveld, and M. Goldfarb, "A preliminary study of the effects of active recovery reflexes on stumble recovery in a swing-assist knee prosthesis," in *Proc. IEEE Int. Conf. Robot. Autom. (ICRA)*, May 2023, pp. 10443–10448.
[35] X. Tian, S. Wang, X. Wang, D. Dong, and Y. Zhang, "Design and control of a compliant Electro-Hydrostatic-Powered ankle prosthesis," *IEEE/ASME Trans. Mechatronics*, vol. 27, no. 5, pp. 2429–2439, Oct. 2022.
[36] T. Yu, A. R. Plummer, P. Iravani, J. Bhatti, S. Zahedi, and D. Moser, "The design, control, and testing of an integrated electrohydrostatic powered ankle prosthesis," *IEEE/ASME Trans. Mechatronics*, vol. 24, no. 3, pp. 1011–1022, Jun. 2019.
[37] M. Puliti, F. Tessari, R. Galluzzi, S. Traverso, A. Tonoli, L. De Michieli, and M. Laffranchi, "A hybrid swing-assistive electro-hydrostatic bionic knee design," in *Proc. 9th IEEE RAS/EMBS Int. Conf. Biomed. Robot. Biomechatronics (BioRob)*, Aug. 2022, pp. 1–7.
[38] M. Puliti, J. Driessen, N. Vitale, F. Tessari, S. Traverso, M. Laffranchi, L. De Michieli, and L. Shtrepi, "Use of metamaterials to reduce acoustic noise emissions from lower limb prostheses: An experimental validation," in *Proc. Int. Conf. Rehabil. Robot. (ICORR)*, Sep. 2023, pp. 1–6.
[39] I. Reginaldi, M. Puliti, A. Bunt, B. Franconi, L. M. Martulli, A. Bernasconi, C. A. Frigo, L. De Michieli, and M. Laffranchi, "Effect of prosthetic mass reduction on metabolic cost and walking symmetry: A case study on lower limbs," in *Proc. 10th IEEE RAS/EMBS Int. Conf. Biomed. Robot. Biomechatronics (BioRob)*, Sep. 2024, pp. 116–121.
[40] M. Puliti, F. Tessari, J. J. M. Driessen, R. Galluzzi, M. Paravano, N. Amati, A. Tonoli, L. D. Michieli, and M. Laffranchi, "Design and validation of a novel partially powered knee prosthesis," in *Proc. IEEE Int. Conf. Adv. Intell. Mechatronics (AIM)*, Jul. 2024, pp. 1609–1614.
[41] M. Grimmer, A. A. Elshamanhory, and P. Beckerle, "Human lower limb joint biomechanics in daily life activities: A literature based requirement analysis for anthropomorphic robot design," *Frontiers Robot. AI*, vol. 7, pp. 1–17, Feb. 2020.
[42] R. Riener, M. Rabuffetti, and C. Frigo, "Stair ascent and descent at different inclinations," *Gait Posture*, vol. 15, no. 1, pp. 32–44, Feb. 2002.
[43] D. A. Winter, *Biomechanics and Motor Control of Human Gait: Normal, Elderly, and Pathological*. Waterloo, ON, Canada: Waterloo Press, 1991.
[44] J. M. Stepien, S. Cavenett, L. Taylor, and M. Crotty, "Activity levels among lower-limb amputees: Self-report versus step activity monitor," *Arch. Phys. Med. Rehabil.*, vol. 88, no. 7, pp. 896–900, Jul. 2007.
[45] E. C. Honert and K. E. Zelik, "Foot and shoe responsible for majority of soft tissue work in early stance of walking," *Human Movement Sci.*, vol. 64, pp. 191–202, Apr. 2019.
[46] P. de Leva, "Adjustments to zatsiorsky-Seluyanov's segment inertia parameters," *J. Biomechanics*, vol. 29, no. 9, pp. 1223–1230, Sep. 1996.
[47] F. Tessari, R. Galluzzi, and N. Amati, "Efficiency-driven design methodology of gerotor hydraulic units," *J. Mech. Design*, vol. 142, no. 6, pp. 063501-1–063501-12, Jun. 2020.
[48] M. Puliti, F. Tessari, R. Galluzzi, A. Tonoli, and N. Amati, "Design methodology of gerotor hydraulic machines for mechatronic applications," in *Proc. ASME I. Mech. Eng. Cong. Express (IMECE)*, Nov. 2021, pp. 1–21.
[49] M. Puliti, R. Galluzzi, F. Tessari, N. Amati, and A. Tonoli, "Energy efficient design of regenerative shock absorbers for automotive suspensions: A multi-objective optimization framework," *Appl. Energy*, vol. 358, Mar. 2024, Art. no. 122542.
[50] Ottobock. *C-leg 4*. Accessed: Oct. 1, 2024. [Online]. Available: https://media.ottobock.com/web-site/prosthetics/lower-limb/c-leg/files/646d878-en-03-1607w.pdf
[51] N. Hogan, "Impedance control: An approach to manipulation: Part II—Implementation," *J. Dyn. Syst., Meas., Control*, vol. 107, no. 1, pp. 8–16, Mar. 1985.
[52] J. T. Lee and M. Goldfarb, "Effect of a swing-assist knee prosthesis on stair ambulation," *IEEE Trans. Neural Syst. Rehabil. Eng.*, vol. 29, pp. 2046–2054, 2021.
[53] D. J. Lura, M. W. Wernke, S. L. Carey, J. T. Kahle, R. M. Miro, and M. J. Highsmith, "Crossover study of amputee stair ascent and descent biomechanics using genium and C-Leg prostheses with comparison to non-amputee control," *Gait Posture*, vol. 58, pp. 103–107, Oct. 2017.
[54] N. J. Rosenblatt, A. Bauer, and M. D. Grabiner, "Relating minimum toe clearance to prospective, self-reported, trip-related stumbles in the community," *Prosthetics Orthotics Int.*, vol. 41, no. 4, pp. 387–392, 2017.
[55] F. Tessari, J. Hermus, R. Sugimoto-Dimitrova, and N. Hogan, "Brownian processes in human motor control support descending neural velocity commands," *Sci. Rep.*, vol. 14, no. 1, pp. 1–15, Apr. 2024.

MARCO PULITI (Student Member, IEEE) was born in Assisi, Italy, in 1996. He received the B.S. degree in mechanical engineering from Università degli studi di Perugia, in 2018, and the M.S. degree in mechatronic engineering from Politecnico di Torino, in 2020.

Since 2020, he has been a Ph.D. Researcher in mechanical engineering with the Rehab Technologies INAIL-IIT Laboratory, Italian Institute of Technology, and the Mechatronics Laboratory, Politecnico di Torino. In 2022, he was a Visiting Researcher with the Center for Rehabilitation Engineering and Assistive Technology, Vanderbilt University, under the supervision of Dr. Michael Goldfarb. His research interests include the control and design of mechatronic systems and fluid dynamics, especially in the fields of rehabilitation and assistive robotics.

FEDERICO TESSARI was born in Bracciano, Italy, in 1991. He received the B.Sc. degree in mechanical engineering from Università degli studi di Roma Tre, in 2014, the M.Sc. degree in mechatronic engineering from Politecnico di Torino, in 2016, and the dual Ph.D. degree in mechanical engineering from Poltecnico di Torino and Italian Institute of Technology, in 2021.

Since 2022, he has been a Postdoctoral Researcher in mechanical engineering with the Newman Laboratory for Biomechanics and Human Rehabilitation, Massachusetts Institute of Technology. His research interests include robotic design and control, biomechanics, human neuro-motor control, and human–machine interaction.

RENATO GALLUZZI (Senior Member, IEEE) was born in Mexico City, Mexico, in 1986. He received the M.Sc. and Ph.D. degrees in mechatronics from Politecnico di Torino, Italy, in 2010 and 2014, respectively. Since 2011, he has been an Active Collaborator of the Mechatronics Laboratory, Politecnico di Torino. He is currently a Research Professor with the School of Engineering and Sciences, Tecnologico de Monterrey, Mexico. He is author of numerous journal publications and conference papers. He also holds inventorship in multiple international patents. His research interests include vibration control and damping systems, power actuators, electric machinery, and energy harvesting.

NICOLA AMATI received the Ph.D. degree in machine design from the Department of Mechanical Engineering, Politecnico di Torino, Turin, Italy, in 2001. He joined the faculty of Politecnico di Torino in the same year, where he is currently a Full Professor with the Mechanical and Aerospace Engineering Department. His research and teaching interests include the analysis, design, and control of electromechanical systems with an emphasis on rotating machinery, active and passive magnetic bearings and dampers, and more-electric systems for automotive applications.

ANDREA TONOLI received the Ph.D. degree in machine design from Politecnico di Torino, 1993. He joined the faculty, in 1994. He is currently a Full Professor with the Mechanical and Aerospace Engineering Department. He was the Director of the Mechatronics Laboratory, Politecnico di Torino, from 2007 to 2011. His research and teaching interests include the analysis, design, and control of electromechanical systems with an emphasis on rotating machinery, active and passive magnetic bearings and dampers, piezoelectric transducers for vibration and motion control, and electromechanical systems for automotive applications.

MATTEO LAFFRANCHI received the master's degree in mechatronic engineering from the Polytechnic University of Turin, in 2006, and the Ph.D. degree in robotics from the University of Sheffield, U.K., in 2011. He is currently a Coordinator of robotics with the Rehab Technologies INAIL-IIT Laboratory, Italian Institute of Technology. Following a brief experience in the automation industry with OSAI A. S., from 2008 to 2011, he has been Research Fellow and Postdoctoral Researcher with the Department of Advanced Robotics (ADVR), Italian Institute of Technology, from 2011 to 2014. Since 2014, he has been with the Rehab Technologies INAIL-IIT Laboratory, with specific focus on the development of novel healthcare robots, particularly robotic prostheses and exoskeletons. He has been manages the activities related to robotics research and product development within the laboratory starting, since 2016.